Reduction of Fiber Alignment Shifts in Semiconductor Laser Module Packaging

Wood-Hi Cheng, *Member, IEEE, Member, OSA*, Maw-Tyan Sheen, Chih-Pen Chien, Hung-Lun Chang, and Jao-Hwa Kuang

***Abstract*—The thermally induced fiber alignment shifts of fiber-solder-ferrule (FSF) joints in laser module packaging have been studied experimentally and numerically. From direct measurements of the metallographic photos with and without temperature cycling, fiber displacement shifts of up to a 0.8 μm were found after undergoing 500 temperature cycles. Experimental results show that the fiber shifts increase as the temperature cycle number and the initial fiber eccentric offset increase. The major cause of fiber shift may come from the plastic solder yielding introduced by the thermal stress variation and the redistribution of the residual stresses during temperature cycling. A finite-element method (FEM) analysis was performed to evaluate the variation of thermal stresses, the distribution of residual stresses, and fiber shifts of the FSF joints. Experimental measurements were in reasonable agreement with the numerical calculations. Both results indicate that the initial offset introduced in the fiber soldering process is a key parameter in causing the thermally-induced fiber shift of FSF joints in laser module packaging. The fiber shift, and hence fiber alignment shift under temperature cycling tests can be reduced significantly if the fiber can be located close to the center of the ferrule.**

***Index Terms*—Fiber alignment shift, finite-element method (FEM), semiconductor laser, semiconductor laser module packaging.**

I. Introduction

TEMPERATURE cycling tests are commonly used in the semiconductor industry to characterize the thermal fatigue failure and to predict reliability of the solder joints in the microelectronics packaging technology [1]. Although other mechanisms, such as vibration, mechanical and thermal shocks, and humidity, may lead to solder joint failure, the primary mechanisms are caused by thermal and residual stresses. For high performance laser-based transmitters in lightwave communication systems, box-type packages of the dual-in-line package (DIP) and butterfly package with fiber pigtails are widely used [2], [3]. Box-type packages allow enough room for an assembly thermoelectric cooler (TEC) component to keep laser operation at a constant temperature. The connected components of the DIP or butterfly package have different material properties and have different coefficients of thermal expansion (CTE), thermal conductivities, Poisson's ratios, and yield strengths. Because of the CTE mismatch, different elongations and contractions take place in the solidification of the solder. These optoelectronic components experience relative movements in the solidification process initially, because a distribution of the residual shear and normal stresses are induced on the solder joint assembly [1]. As a result of temperature cycles, the fluctuation of the thermal stress may introduce some thermal yielding locally and redistribute the residual stresses in the solder joints. An alignment shift of the fiber in the DIP or butterfly package may be accumulated from successive temperature cycles. Generally, this fiber alignment shift of a DIP or a butterfly package is very small, in the micron range. In a typical single-mode fiber application, if the fiber alignment shift induced by the temperature cycling is even a few micrometers, up to a 50% loss in coupled power may be incurred, and result in performance degradation of the packaged lasers. Therefore, how to minimize the fiber alignment shift in the temperature cycling test is one of the key research topics for the study of yield and reliability in optoelectronic packaging applications.

There are so many components in the DIP or butterfly packages that it is difficulty to identify the specific components which should responsible for the fiber alignment shift under temperature cycling tests. Furthermore, the order of the fiber alignment shift is quite small, in the micron range. It is also a difficult task to find the proper reference system to measure the fiber alignment shift in the DIP or butterfly packages. In this work, we have studied the fiber alignment shift introduced in the key component, the fiber-solder-ferrule (FSF) assembly in the DIP. A novel metallographic technique using scratch lines in the FSF joints is used as the reference marks for the fiber alignment shift measurements.

The purpose of this study is to provide useful design guidance for understanding and evaluating the possible fiber alignment shifts under the temperature cycling tests for optical module packaging applications. The results of this work have led to fabricating reliable and high-performance laser module packages for use in lightwave communication system applications. The following sections of this paper are organized as follows. Section II describes the package construction and experimental procedure. The measurement results of fiber shifts are presented in Section III. Section IV describes the FEM model, and the results of numerical simulations are presented in Section V. A discussion and brief summary are given in Section VI.

Manuscript received November 23, 1999; revised February 28, 2000. This work was supported in part by National Science Council, R.O.C., under Contract NSC 89-2215-E-110-009.

W.-H. Cheng and C.-P. Chien are with the Institute of Electro-Optical Engineering, National Sun Yat-sen University, Kaohsiung, Taiwan 80424, R.O.C.

M.-T. Sheen and J.-H. Kuang are with the Department of Mechanical Engineering, National Sun Yat-sen University, Kaohsiung, Taiwan 80424, R.O.C.

H.-L. Chang is with Chunghwa Telecom Laboratories, Yang-Mei, Taoyuan, Taiwan, R.O.C.

Publisher Item Identifier S 0733-8724(00)05080-5.

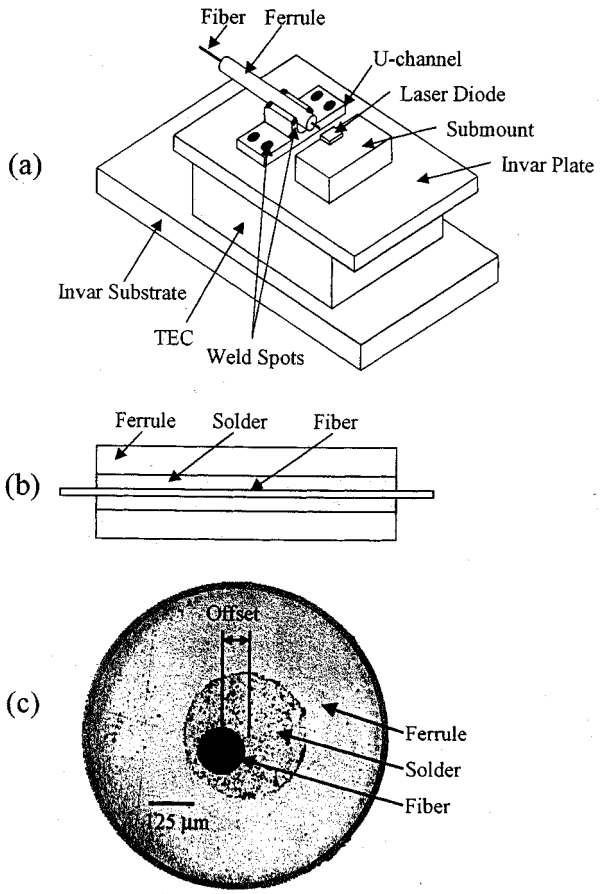

Fig. 1. (a) Schematic diagram of the top view of a DIP showing the pigtail fiber to laser connection, (b) a ferrule-solder-fiber joint, (c) a metallographic photo showing the ferrule, solder, fiber and fiber eccentric offset.

II. Package Construction and Experimental Procedure

A. Package Construction

A DIP laser module construction consisted of a 1.3 μm laser, the Invar housing materials, a TEC, and a single-mode fiber, as shown in Fig. 1(a). Invar [4] and Kovar [5] with their very low CTE have been frequently used as the housing material for optoelectronic packaging. In this work, the Invar plate and u-channel of the Invar housing materials, and Invar ferrule of DIP laser module with the very low CTE of $1.5 \times 10^{-6}/°\text{C}$ were chosen to minimize thermal stresses and strains [4], [6], [7].

In the process of fabricating a DIP, a dual-beam laser welding system was used to connect the pigtail fiber assembly to the semiconductor laser. There were a total of eight welded spots on the laser-welded Invar tube-to-u-channel and u-channel-to-Invar plate joints as shown in Fig. 1(a). Details on the welding process of DIP laser package were found elsewhere [8], [9]. To enhance the solderability for chip and wire bonding, the Invar housing material was coated with Au thin film. In a DIP construction, the fiber-to-Invar ferrule and the submount-to-Invar plate assemblies were solder joints, while the Invar ferrule-to-u-channel and the u-channel-to-Invar plate assemblies were weld joints. Both solder joints for good adhesion and weld joints for high strength in the same Invar housing materials are essential for ensuring good reliability in optoelectronic packages [8].

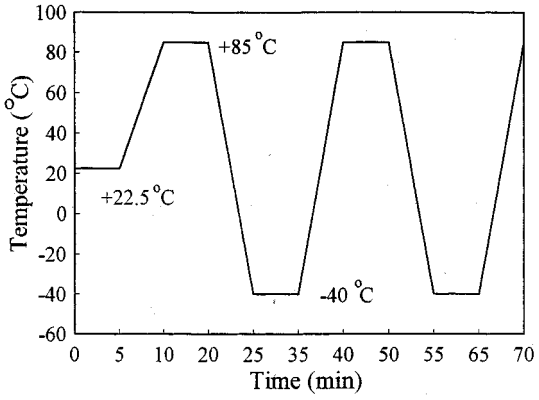

Fig. 2. A process of the temperature cycling test from -40 °C to $+85$ °C.

B. Fiber-Solder-Ferrule (FSF) Assembly

The ends of metallized optical fibers are often sealed by soldering into ferrules prior to use in laser welding processes for joining between the ferrule and clip [7]–[9]. Obviously, the solder joint in an FSF assembly must be able to withstand higher thermal stress under temperature cycling and aging conditions. Various types of solder, such as Sn/Pb, In, Au, and Sn/Au, have been used for sealing between the metallized fiber and metal support ferrule [7]. In this work, the solder joint in an FSF assembly consisted of a metallized fiber, an Sn(63)/Pb(37) solder ($T_m = 183$°C), and an Invar ferrule, as shown in Fig. 1 (b). The metallized fiber was fabricated by coating with Ni and Au using sputting technique. The metallized fiber was then processed through inside the Invar ferrule. Finally, the FSF joint was assembled by heating the solder of Sn/Pb at 200°C. Due to the solidification shrinkage of the solder in the FSF assembly, the fiber is difficult to locate at the center of the ferrule tube. An undesired eccentric offset can be introduced. In this article, the fiber eccentric offset of an FSF assembly was specified by the center distance between the fiber and the ferrule, as shown in Fig. 1 (c).

C. Temperature Cycling Test

Following the Bellcore Reliability Assurance Practices of TA-TSY-000 983 [10], the process of the temperature cycling test is shown in Fig. 2. During the temperature cycling test, the temperature was changed from $-$ 40 °C to 85°C within a three-hour cycle. The ramp rate was greater than 10°C/min and the dwell time was 30 min for a total of 500 cycles. The fiber shifts were measured and recorded for every 100 cycles.

III. Measurements and Results

A. Fiber Center Shift Measurements

The standard procedures of the metallographic preparation are the sample sectioning, mounting, grinding and polishing, chemical etching, microscope examination, and measurements [11]. The scratch lines on an FSF assembly were due to grinding and polishing processes in metallographic preparation, as shown in Fig. 3. The reference marks were obtained by choosing the intersection of two scratch lines. Five reference marks O_1, O_2, O_3, O_4, and O_5 were chosen as the fix references located on

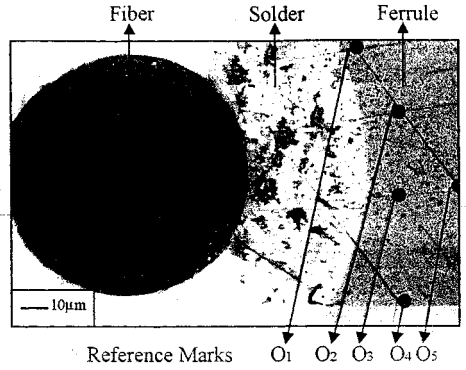

Fig. 3. A metallographic photo showing the ferrule, solder, and fiber with the reference marks.

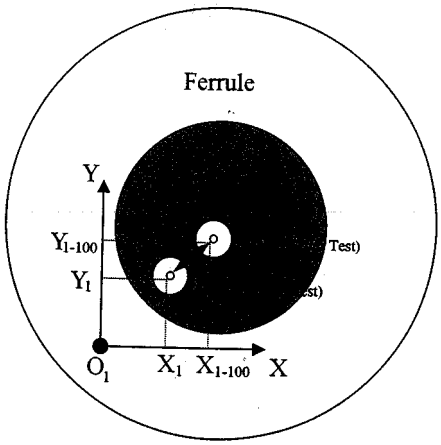

Fig. 4. The fiber center shift calculation of a ferrule-solder-fiber joint.

the ferrule to specify the fiber center shifts. In this study, due to the very low CTE of the Invar material, the shape and the size of the ferrule was assumed to be temperature invariant in the temperature cycling test. By defining the reference marks on the ferrule as a fixed system and the center of the fiber as a moving point, the thermally induced fiber shifts then could be determined from the distance variation between the center of the fiber and the five fixed reference mark points in the ferrule. A shift in the micron range can be measured with a powerful microscope. As shown in Fig. 4, the reference mark O_1 is used to determine the fiber center shift ΔS. The fiber center shift ΔS_1 after 100 temperature cycles can be approximated by

$$\Delta S_1 = [(X_{1-100} - X_1)^2 + (Y_{1-100} - Y_1)^2]^{1/2} \qquad (1)$$

where X_1 and Y_1, $X_{1\text{-}100}$ and $Y_{1\text{-}100}$ are coordinates of the center of the fiber before and after 100 temperature cycling, respectively. An average of five measurements of ΔS_1, ΔS_2, ΔS_3, ΔS_4, and ΔS_5 based on different reference marks of O_1, O_2, O_3, O_4, and O_5, respectively, were used to specify the fiber center shift.

In order to investigate the effect of the initial offset on the thermal alignment shift, five FSF assemblies with different offsets are used for temperature cycling tests. During the test, the surrounding temperature in a heating chamber was changed from -40 to 85°C within a three-hour cycle. The fiber center

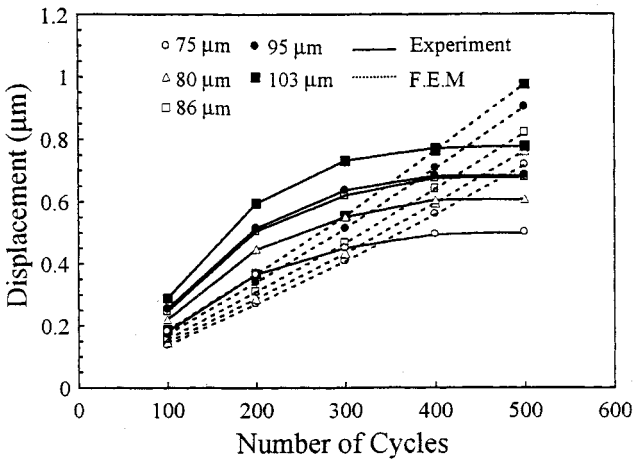

Fig. 5. The measured and calculated fiber displacement shifts as a function of the cycle number for different fiber eccentric offsets.

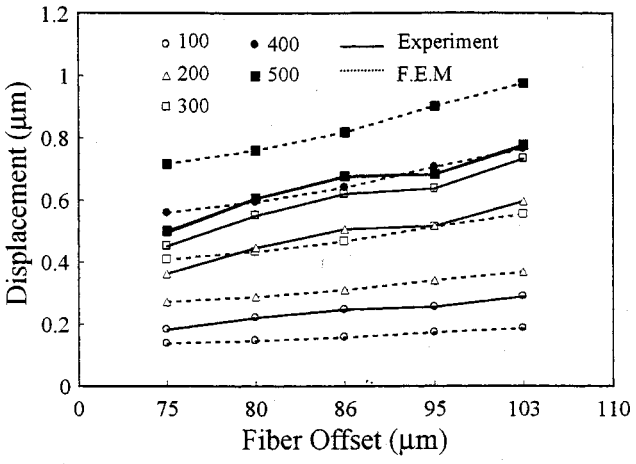

Fig. 6. The measured and calculated fiber displacement shifts as a function of the fiber eccentric offset for different cycle numbers.

shifts were measured from the metallographic photos with and without the temperature cycling tests for every 100 cycles. The temperature cycling tests were measured up to 500 cycles.

B. Results

Five FSF assemblies with different fiber eccentric offsets of 75, 80, 86, 95, and 103 μm are used for fiber center shift measurements undergoing different temperature cycles. Measured results, as shown in Fig. 5, indicate that the fiber shift is dependent upon the cycle number and the initial eccentric offset. The fiber shifts increased as the cycle number increased, and then became steady after 300 cycles. This fiber permanent shift may cumulate from the thermal yielding and the redistribution of the residual stresses within the solder. The combined thermal and residual stresses will push the fiber toward the center of the ferrule tube, as observed in metallographic photo. A fiber shift up to 0.8 μm was observed after 500 cycles.

Fig. 6 shows the measured fiber displacements as a function of the fiber eccentric offset for different cycle number numbers.

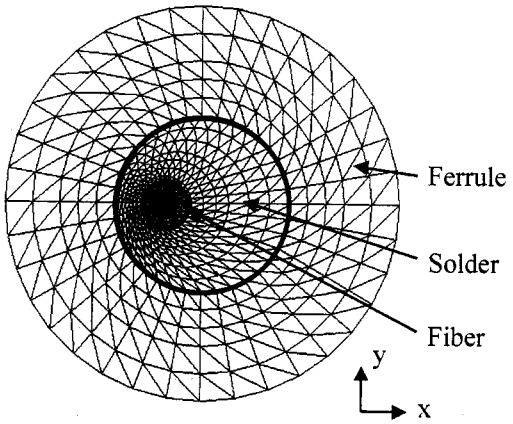

Fig. 7. A representative FEM model of an FSF joint with the fiber near the center.

The fiber displacements increased as the fiber eccentric offset increased. This may be due to a severe thermal stresses fluctuation and the redistribution of the residual stresses around the solder as the fiber offset increases. Fig. 6 indicates that the FSF joints with smaller fiber offset (75 μm) exhibit a 1.5 times less fiber alignment shift than those of the FSF joints with larger fiber offset (103 μm). Therefore, it clearly shows that in the process of an FSF assembly for laser module packaging, the fiber should be located close to the center of ferrule to reduce the initial offset effect.

IV. Finite-Element Method (FEM)

A. Finite-Element Model

Numerical calculations of the fluctuation of the thermal stresses, the distribution of the residual stresses, and fiber center shifts in the FSF joint during temperature cycling were performed using commercial MARC [12] and MENTAT [13] finite element packages. A plane strain triangular element model with the temperature-varied material properties was employed in this work. The diameters of the ferrule, solder, and fiber were 0.9, 0.4, and 0.125 mm, respectively. A mesh with 685 nodes, and 360, 432, and 540 isotropic triangle elements for ferrule, solder, and fiber, respectively, was employed for the simulation. Fig. 7 shows a representative FEM model of an FSF joint with the fiber near the center. Due to the geometry of the FSF assembly as shown in Fig. 1, a cross section of the solder area was meshed for the FEM simulation. Meshes with triangle type elements were created with an automatic mesh generator.

B. Material Properties

The physical constants and material properties of Inver ferrule, PbSn solder, and fiber at room temperature used in the simulation are listed in Tables I and II, respectively [14]. The values of the CTE, Young's modules, yield strength, Poisson's ratios, thermal conductivity, and specific heat are considered temperature dependent. Because of the limit of the experimental data available for the Inver, the temperature dependence of these material properties near the melting temperature region were assumed to have a tendency similar to that of stainless steel (SS) 304L. The material properties as a function of temperature for SS 304L were obtained from the Metals Handbook [15].

TABLE I
Physical Constants of the Young's Modulus, Poission Ratio, and CTE [14]

Material	Invar	Sn(63)/Pb(37)	Fiber
Young's module (Gpa)	141	32	8
Yield strength (MPa)	275.6	34.43	234.4
Poission ratio	0.3	0.4	0.23
Thermal expansion Coefficient (μm/m^{o}C)	0.7	24.7	0.55

TABLE II
Material Properties of Thermal Conductivity, Specific Heat, and Mass Density

Material	Invar	Sn(63)/Pb(37)	Fiber
Thermal conductivity (W/mK)	16.4	50.6	2
Specific heat (J/kg^{o}C)	258.6	128	840
Mass density (Kg/m^{3})	8080	1080	2800

C. Boundary and Initial Conditions

In this FEM model, the boundary nodes were considered free except at the most right edge point. To calculate the residual stresses, the solder was assumed to be heated from the ambient temperature 22.5 to 195 °C in 20 ms initially and then the whole ferrule system was cooled down to ambient temperature with the assumption of free convection. The cooling time was about 180 ms in this study. The melting temperature of the solder in the melting area was 183 °C. The residual stresses caused from the CTE mismatch and the solidification shrinkage of the solder were calculated. In the simulation of the temperature cycling test, the surrounding temperature varied from -40 to 85 °C within a three-hour cycle [10].

D. FEM Calculations

The modeling approach performed in this study is based on a nonlinear FEM to describe the total strain in the FSF joint. The constitutive model of total strains in the solder joint is given by [16]

$$\varepsilon_{ij} = \varepsilon_{ij}^{e} + \varepsilon_{ij}^{p} + \varepsilon_{ij}^{T} \tag{2}$$

where $\varepsilon_{ij}^{e}, \varepsilon_{ij}^{T}, \varepsilon_{ij}^{p}$ denote the corresponding elastic, plastic, and thermal components of the total strain. According to the generalized Hooke's law for isotropic materials [17], the elastic strain is expressed as

$$\varepsilon_{ij}^{e} = \frac{1+\nu}{E}\sigma_{ij} - \frac{\nu}{E}\sigma_{kk}\delta_{ij} \tag{3}$$

where ν, E, σ_{ij}, σ_{kk}, and δ_{ij}, are the Possion's ratio, the Young's modulus, the stress tensor at the ij component, the stress tensor at the kk component, and the Kronecker delta,

respectively. The stress tensor σ_{ij} can be obtained from the equation of equilibrium and is given by [17]

$$\sigma_{ij,j} + \rho b_i = 0 \quad \text{with } \sigma_{ij} = \sigma_{ji} \tag{4}$$

where ρ, b_i and, $\sigma_{ij,j}$ are the material density, the body force, and the derivative of stress tensor, respectively.

To calculate the plastic strain, the stress-strain equations for von Mises material with the associated mixed-hardening rule has been used and expressed as [17]

$$f(\sigma_{ij} - \alpha_{ij}, K) = 3/2 S_{ij} S_{ij} - \sigma_e^2(\varepsilon_p) = 0 \tag{5}$$

where σ_{ij}, K, S_{ij}, ε_p, σ_e are the stress tensor, the hardening parameter, the deviatoric reduced stress tensor, the reduced effective plastic strain, and the reduced effective plastic strain, respectively.

It is well known that the thermal strain versus temperature behavior is represented as [18]

$$\varepsilon_{ij}^T = \alpha T \delta_{ij} \tag{6}$$

where α, ΔT, and δ_{ij} are the thermal expansion coefficient, the temperature difference, and the Kronecker delta, respectively.

In this study of the FEM model, the theory of coupled thermo-elastoplasticity is adopted to solve the stress distribution in solder joints. Combining (3), (4), (5) and (6), the stress $\{d\sigma\}$-strain $\{d\varepsilon\}$ relationship in this coupled thermo-elastoplasticity model is expressed as [19]

$$\{d\sigma\} = [C^{ep}][d\varepsilon] - [C^{th}]\, dT \tag{7}$$

where $[C^{ep}]$, $[C^{th}]$, dT are the matrix of elastoplasticity moduli, the matrix of thermal moduli, and the temperature difference, respectively. An ambient temperature of 22.5 °C is used as the temperature reference in this study.

The temperature of components of a fiber-solder-ferrule system, T, in (2) to (7) can be determined by a two-dimension heat conduction equation and is given by [20]

$$\nabla \cdot (k \nabla T) = C \cdot \rho \cdot \frac{\partial T}{\partial t} - Q \tag{8}$$

with the heat convection condition on the free surface boundary

$$-K \frac{\partial T}{\partial n} = h(T - T_s) \tag{9}$$

where k, C, ρ, Q, h, n, and T_s are the thermal conductivity, the specific heat, the density, the heat source, the convection heat transfer coefficient, the unit vector normal to the melting boundary, and the ambient temperature, respectively.

Using (2)–(9) and the commercial MARC [12] and MENTAT [13] finite element packages, the distributions of residual stresses, thermal stresses, and hence the fiber displacement shifts in the FSF joints were obtained and are presented in Section V.

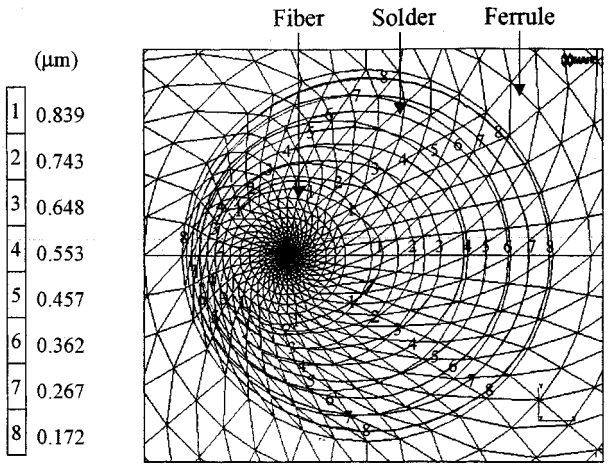

Fig. 8. An equivalent fiber displacement of an FSF joint with an initial 86 μm fiber eccentric offset.

V. FEM Simulation Results

Fig. 8 shows the variation of accumulated fiber thermal shifts after 500 temperature cycling with an initial 86 μm fiber eccentric offset of the FEM model. Results indicate that the thermal shifts are varied from 0.17 to 0.84 μm near the fiber. The largest thermal shift up to 0.84 μm was found near the fiber boundary. This thermal shift may be caused by the local thermal yielding and the redistribution of the residual stresses within the solder.

Results in Fig. 5 also show that the simulated fiber shifts depend upon the cycle number and the initial fiber eccentric offsets. Up to a 1-μm fiber shift was predicted after 500 temperature cycling tests. Comparison with the measured fiber shifts in Fig. 5 indicates that results calculated from the proposed FEM model are in reasonable agreement with results measured experimentally. Clearly, detailed knowledge the phenomenon of thermal alignment shift of a fiber-solder-ferrule undergoing a temperature cycling test is complicate. Nevertheless, from the analyzes of the stress distribution variations proposed by the FEM model, it is believed that one of the major causes of fiber alignment shift experienced in the temperature cycling test is due to the redistribution of the residual stresses within the solder. However, the simulated results of fiber shifts did not become steady after 300 cycles. The different variation tendency between the calculated data and the measured data may come from the ignorance of the creep phenomenon [16] in the temperature cycling tests. To provide an understanding about the fiber alignment shift of a fiber-solder-ferrule joint, detailed knowledge of the combined effect of the residual stresses and creep effect within the solder is necessary and will be pursued in a separate study.

In Fig. 6, results show that the variation tendency of the simulated fiber shifts and the measured fiber shifts is similar, both are dependent upon the fiber initial eccentric offset. The magnitudes of the calculated and the measured fiber shifts are also in a reasonable agreement. Results in Figs. (5) and (6) indicate that the proposed FEM model is effective for predicting the thermally induced fiber shifts of FSF joints. Both experimental and

numerical results clearly show that in the process of an FSF assembly for laser module packaging, the fiber should be located as close as possible to the ferrule center to reduce the undesired thermally-induced alignment shift.

VI. Discussion and Conclusion

In this study, we have presented the experimental and numerical results of the thermally-induced fiber alignment shifts of fiber-solder-ferrule (FSF) joints in semiconductor laser module packaging. These results can be used for fabricating reliable and high-performance laser module packages for use in lightwave communication system applications. The following conclusions can be drawn from the analyzes which have been presented here:

1) Up to a 0.8 μm fiber alignment shift of FSF joints is found after 500 temperature cycling tests. The fiber alignment shifts are increased with the temperature cycles and the initial fiber eccentric offset introduced in the fiber soldering process.
2) A larger initial fiber offset (103 μm) may introduce a 1.5 times alignment shift than those of the FSF joints with a smaller initial fiber offset (75 μm). Therefore, in process of a FSF assembly for laser module packaging, the fiber needs to be soldered near the center of ferrule in order to reduce the initial fiber eccentric offset, and hence reduce the thermal alignment shift under temperature cycling tests.
3) The major cause of fiber alignment shifts may come from the local thermal yielding and the redistribution of the residual stresses within the solder during temperature cycling tests. The high temperature creep phenomenon within the solder may also have significant influence on the fiber thermal shifts.
4) A proposed thermo-elastoplasticity coupled FEM model is employed to simulate distributions of thermal stresses, residual stresses, and the fiber alignment shifts under different number of temperature cycles.
5) Numerical results are in reasonable agreement with experimental results. This indicates that the proposed FEM model is an effective method for predicting the fiber alignment shifts in soldering joints.

Acknowledgment

The authors would like to thank S. C. Wang, C. Wang, and C. M. Wang of Chunghwa Telecom Laboratories, Taiwan, R.O.C., for their stimulation discussion and valuable suggestions. The authors would also like to thank K. C. Hsieh, J. C. Chen, and G. L. Wang of National Sun Yat-sen University for their technical support of this work.

References

[1] C. Basaran and R. Chandaroy, "Finite element simulation of the temperature cycling tests," *IEEE Trans. Comp., Hybrids, Manufact. Technol.*, vol. 20, pp. 530–536, 1997.
[2] D. S. Alles, "Trends in laser packaging," in *Proc. 40th ECTC*, 1990, pp. 185–192.
[3] J. H. Kuang, M. T. Sheen, S. C. Wang, C. H. Chen, and W. H. Cheng, "Crack formation mechanism in laser-welded Au-coated Invar materials for semiconductor laser packaging," *IEEE Trans. Comp., Hybrids, Manufact. Technol.*, pp. 94–100, 1999.
[4] *Metals Handbook: Low-Expansion Alloys*, 8th ed., vol. 8, ASM, 1973, pp. 266–267.
[5] *Kovar Alloy Handbook*, Westinghouse Electric Co., PA, 1971.
[6] R. Chanchani and P. M. Hall, "Temperature dependence of thermal expansion of ceramics and metals for electronic packages," *IEEE Trans. Comp., Hybrids, Manufact. Technol.*, vol. 13, pp. 743–750, 1990.
[7] E. Suhir, "Thermally induced stresses in an optical glass fiber soldered into a ferrule," *J. Lightwave Techol.*, vol. 12, pp. 1766–1770, 1994.
[8] W. H. Cheng, Y. D. Yang, S. C. Wang, S. Chi, M. T. Sheen, and J. H. Kuang, "Effect of Au thickness on laser beam penetration in semiconductor laser packages," *IEEE Trans. Comp., Hybrids, Manufact. Technol.*, vol. 20, pp. 396–402, 1997.
[9] W. H. Cheng, M. T. Sheen, J. H. Kuang, and C. H. Chen, "The principle cause of crack defects in optoelectronic materials with phosphorus-containing underlayer," *J. Electron. Mater.*, vol. 28, pp. 50–56, 1999.
[10] "Bellcore Reliability Assurance Practices for Optoelectronic Devices in Loop Applications,", pt. 1, TA-TSY-000 983, Jan. 1990.
[11] W. H. Cheng, W. H. Wang, and J. C. Chen, "Defect formation mechanisms in laser welding technique for semiconductor laser packaging," *IEEE Trans. Comp., Hybrids, Manufact. Technol.*, vol. 19, pp. 764–769, 1996.
[12] *User Guide*, MARC 6.3, MARC Analysis Research Corporation, Palo Alto, CA, 1996.
[13] *User Guide*, MENTAL II, MARC Analysis Research Corporation, Palo Alto, CA, 1996.
[14] J. H. Lau and Y. H. Pao, *Solder Joint Reliability of BGA, CSP, Flip Chips, and Fine Pitxh SMT Assemblies*. New York: McGraw-Hill, 1997, ch. 4.
[15] *Metals Handbook*, 8th ed., ASM, Metals Park, OH, 1973, pp. 2–73 and 2–200.
[16] T. Y. Pan, "Thermal cycling induced plastic deformation in solder joints—Part 1: Accumulated deformation in surface mount joints," *J. Electronic Packaging*, vol. 113, pp. 8–15, 1991.
[17] W. F. Chen and D. J. Han, *Plasticity for Structure Engineers* Gau Lih, Taiwan, ch. 3 and 5.
[18] W. B. Bickford, *Mechanics of Solids-Concepts and Applications*. Australia: Richard D. Irwin, 1993, ch. 4.
[19] K. J. Bathe, *Finite Element Procedures*. Englewood, Cliffs, NJ: Prentice-Hall International, 1996, ch. 6.
[20] F. P. Incropera and D. P. DeWitt, *Fundamentals of Heat and Mass Transfer*. New York: Wiley, 1996, ch. 2.

Wood-Hi Cheng (M'95) was born in Changhua, Taiwan, R.O.C., on June 3, 1944. He received the Ph.D. degree in physics from Oklahoma State University, Stillwater, in 1978.

He is a Professor and Director of the Institute of Electro-Optical Engineering, National Sun Yat-sen University, Kaosiung, Taiwan, R.O.C. From 1991 to 1994, he was an Optoelectronic Packaging Manager at Tacan Corporation. Carlsbad, CA. From 1984 to 1991, he was a Principal Design Engineer at Rockwell International, Newbury Park, CA. From 1980 to 1984, he was a Research Engineer at General Optronics, Edison, NJ, and from 1978 to 1980, he was a Research Associate at Telecommunication Laboratories, Taiwan. His research and development activities have been focused on the design and fabrication of high-speed semiconductor lasers for lightwave communications, highly efficient light coupling from lasers and LED's into fibers, fiber couplers, characterization of III–V semiconductors materials, and optoelectronic packaging. His current research interests are failure analysis and finite-element method for semiconductor laser packaging, novel material for high-density WDM, and high-speed semiconductor lasers for analog and digital lightwave transmission systems. He served as a consultant for Chunghwa Telecom Laboratories, Opto-Electronics and System Laboratories, and Chung-Shan Institute of Science and Technology, all from Taiwan.

He is a member of the Optical Society of America (OSA), the Photonics Society of Chinese-Americans, and serves as a Chair for the IEEE Lasers and Electro-Optics Society (LEOS), Taipei Chapter.

Maw-Tyan Sheen received the B.S. and M.S. degrees in mechanical engineering from National Cheng Kung University, Tainan, Taiwan, R.O.C., in 1989 and 1994, respectively, where he is currently pursuing the Ph.D. degree.

From 1994 to 1995, he was a Teacher at Yang-Ming High School, Tainan. His research interests are optoelectronic packaging, laser welding technology for low-cost laser modules, and finite-element method for laser packaging.

Chih-Pen Chien received the B.S. degree in mechanical engineering from National Taiwan University of Science and Technology, Taipei, Taiwan, R.O.C., in 1996, and the M.S. degree in electro-optical engineering, from National Sun Yat-sen University, Kaoshiung, Taiwan, R.O.C., in 1999.

He currently is an Optoelectronic Engineering Project Leader at Daffo Electric Corporation, Taipei, Taiwan.

Hung-Lun Chang received the B.S. degree in electrophysics, and the Ph.D. degree in electro-optical engineering, all from National Chiao Tung University, Hsinchu, Taiwan, R.O.C., in 1986, and 1991, respectively.

Since 1991, he has been working as an Associate Researcher and Project Manager at the Applied Research Laboratory, Chunghwa Telecom Laboratories, Taoyan, Taiwan. His primary research interests are the packaging technologies of optoelectronic components and modules for telecommunication applications.

Jao-Hwa Kung received the B.S. degree in mechanical engineering from National Cheng Kung University, Tainan, Taiwan, R.O.C., in 1970 and the Ph.D. degree in mechanical engineering from the University of Cincinnati, Cincinnati, OH, in 1983.

He is a Professor of the Department of Mechanical Engineering, National Sun Yat-sen University, Kaoshiung, Taiwan. His primary research focuses in the area of dynamic stress analysis.